nature photonics

LETTERS

https://doi.org/10.1038/s41566-021-00943-3

Check for updates

OPEN

Observation-dependent suppression and enhancement of two-photon coincidences by tailored losses

Max Ehrhardt, Matthias Heinrich and Alexander Szameit ✉

The ability of indistinguishable particles to interfere with one another is a core principle of quantum mechanics. The interplay of interference and particles exchange statistics[1–4] gives rise to the Hong–Ou–Mandel (HOM) effect[5], where the bunching of bosons suppresses two-particle coincidences between the output ports of a balanced beamsplitter. Conversely, fermionic anti-bunching can yield up to a twofold enhancement of coincidences compared to the baseline of distinguishable particles. As such, the emergence of dips or peaks in the HOM effect may appear indicative of the particles' bosonic/fermionic nature. Here, we demonstrate experimentally that the coincidence statistics of boson pairs can be seamlessly tuned from full suppression to enhancement by an appropriate choice of the observation basis. Our photonic setting leverages birefringent couplers[6] to introduce differential dissipation in the photons' polarization. In contrast to previous work[7–9], the mechanism underpinning this unusual behaviour does not act on individual phases accumulated by pairs of particles along specific paths, but instead allows them to jointly evade losses as indistinguishable photons are prevented from inhabiting orthogonal modes. Our findings reveal a new approach to harnessing non-Hermitian settings for the manipulation of multi-particle quantum states and as functional elements in quantum simulation.

Energy exchange with the environment is an inescapable feature for any physical system. As such, the fundamental assumption of Hermiticity, as convenient as it may be, for example, in the theoretical description of quantum systems, necessarily constitutes an approximation. Historically, non-Hermitian characteristics tended to be neglected as a matter of course, while the utility of their twofold appearance as gain and loss was primarily seen in their capacity for mutual cancellation. Yet, sparked by the ground-breaking work of Bender and Boettcher on parity-time (PT) symmetry[10] and its subsequent adaptation to optical settings[11], a slew of works[12] have revealed fascinating features arising from the complex interplay of gain and loss, for example, in non-orthogonal eigenmodes[13], peculiar transport properties[14], loss-induced transparency[15] and unidirectional invisibility[16] as well as exceptional points[16,17] with enhanced response[18], PT-symmetric lasers[19,20] and even light-funnelling[21]. However, although gain and loss are readily incorporated into classical optics as a complex-valued refractive index profile, the consequences of changing the number of particles pose fundamental constraints on how these concepts can be brought to bear on genuine quantum states of light[22]. Fortunately, inadvertently introducing additional quantum noise can be avoided by entirely passive configurations. For example, quasi-PT-symmetric loss distributions in directional couplers have been shown to systematically accelerate the onset of fully destructive two-photon quantum interference[23]. Along similar lines, lossy beamsplitters[7], opaque scattering media[8], non-unitary metasurfaces[24] or photonically implemented quantum decay processes[9] may enhance two-photon coincidence rates for indistinguishable photon pairs, yielding a peak instead of the conventional dip in the Hong–Ou–Mandel (HOM) experiment, which in Hermitian systems would be indicative of fermionic anti-bunching behaviour.

In this Letter we experimentally demonstrate that, even if loss-induced anti-bunching in the form of a HOM peak is observed, the photons' bosonic characteristics of destructive quantum interference—a HOM dip—can nevertheless be retained by an appropriate choice of the observation basis. To this end, we implement non-Hermitian two-port couplers based on femtosecond laser-written birefringent waveguides[25], where polarization oscillations of photons play the role of continuous coupling between orthogonal polarization bases,[6] and extended ancillary arrays provide the desired amounts of loss[26,27] through polarization-sensitive coupling[28]. Notably, indistinguishable photons are known for being able to partially evade lossy domains in unison[29], which affects the transition probability of photon pairs depending on their degree of indistinguishability, resulting in an apparent enhancement of the contribution of indistinguishable photon pairs (Fig. 1a). Regardless of the number of transmitted photon pairs however, bunching can be enforced for indistinguishable photons through the choice of the observation basis. As outlined in Fig. 1b, bunched photon pairs cannot be detected via coincidence measurement in specific bases, allowing for a suppression of their registered coincidences C_{ind} compared to the baseline C_{dis} of distinguishable photon pairs that remain unaffected (Fig. 1c). We harness a combination of these two effects to induce a continuous transition from enhancement (that is, a HOM peak) in one polarization basis set to full suppression (a HOM dip) in its counterpart that has been rotated by 45° (Fig. 1d), whereas the conventional HOM dip as a sign of bosonic two-photon interference on a balanced beamsplitter remains strictly basis-independent (Fig. 1e). To gain more detailed insights into these dynamics, we study the HOM patterns for representative basis orientations associated with visibilities of $\nu = C_{\mathrm{ind}}/C_{\mathrm{dis}} - 1 < 0$ (that is, the conventional HOM dip) to peaks ($\nu > 0$). Furthermore, by experimentally probing the influence of the paths taken by photon pairs through the sample, we show that HOM interference actually remains unaffected by the specific phases accumulated by their constituent particles, revealing an entirely new approach to systematically tailor photon coincidence statistics beyond techniques based on selective transmission[24].

Institute for Physics, University of Rostock, Rostock, Germany. ✉e-mail: alexander.szameit@uni-rostock.de

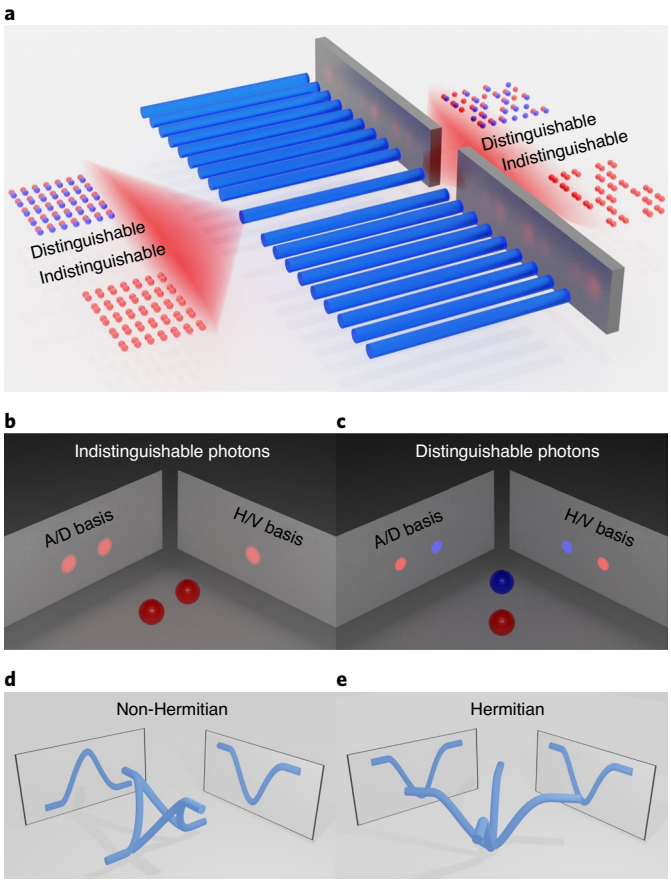

Fig. 1 | Propagation and coincidence detection of photon pairs in lossy systems. a, When pairs of distinguishable (red/blue) and indistinguishable (red/red) photons are launched in identical quantities, lossy regions (here represented by the coupling to ancillary arrays) affect the correlations of distinguishable photon pairs more strongly. In turn, the transmission of indistinguishable photon pairs is effectively enhanced. **b**, Illustration of observation-dependent coincidence detection for indistinguishable photon pairs. In the observation in basis 1, the photons inhabit different states, allowing them to jointly register in a coincidence measurement. By contrast, when the photons occur in the same state (bunching), they are rendered invisible to coincidence measurement between the states spanning basis 2. **c**, Distinguishable photons do not occur in bunched states, allowing them to be measured as coincidences independently of the measurement basis, as long as neither of them has been annihilated. **d**, Schematic geometric interpretation of the basis-dependent outcome of the HOM experiment in a non-Hermitian polarization coupler. Depending on the perspective, the structure may be perceived either as a dip or a peak, respectively. **e**, By contrast, for the conventional Hermitian structure, the appearance remains invariant against rotations of the observation basis.

Our setting is based on birefringent waveguides, which can be described with a pair of propagation constants, β_H and β_V, associated with photons polarized horizontally and vertically, in line with the structure's principal axes (Fig. 2a). As demonstrated recently, such waveguides can be employed as a directional coupler in polarization space[6]. Viewed through this lens, they promote a periodic, coherent transfer of excitation between the diagonal state $|D\rangle = (|V\rangle + |H\rangle)/\sqrt{2}$ and the anti-diagonal one $|A\rangle = (|V\rangle - |H\rangle)/\sqrt{2}$ upon propagation along the longitudinal coordinate z. Although both $|D\rangle$ and $|A\rangle$ evolve with the mean propagation constant $\bar{\beta} = (\beta_V + \beta_H)/2$, the rate of coupling between them is governed by the mismatch $\Delta\beta = (\beta_V - \beta_H)/2$, that is the strength of birefringence. To impose dissipation to the system, we employ (spatial) coupling to ancillary waveguide arrays placed in its vicinity (Fig. 2b). Although no actual absorption is introduced, the presence of these extended arrangements of similarly birefringent waveguides provides a flexible means to drain light from the states $|H\rangle$ and $|V\rangle$ with polarization-dependent coupling strengths[28] C_H and C_V. Once photons have tunnelled out of the target waveguide, the comparatively stronger coupling within the arrays immediately conveys the photons to the sides by means of ballistic discrete diffraction[27]. Although the resulting polarization-sensitive loss rates γ_H and γ_V indeed selectively affect the evolution of the initial amplitudes $\alpha_{H/V}$ ($\alpha_H^2 + \alpha_V^2 = 1$) of a single-photon state

$$|\psi(z)\rangle = \alpha_H e^{-\gamma_H z} e^{-i\beta_H z}|H\rangle + \alpha_V e^{-\gamma_V z} e^{-i\beta_V z}|V\rangle \qquad (1)$$

when described as a superposition of the polarization eigenstates $|H\rangle$ and $|V\rangle$, the mean loss rate $\bar{\gamma} = (\gamma_H + \gamma_V)/2$ represents the balanced global loss rate imposed on the states $|D\rangle$ and $|A\rangle$. In turn, the difference in the individual loss rates $\Delta\gamma = (\gamma_H - \gamma_V)/2$ appears as the imaginary part in their coupling rate (Fig. 2c).

As shown in Fig. 3a, horizontally and vertically polarized excitations of the target waveguide are indeed attenuated at markedly different rates, as confirmed by tight-binding simulations. Notably, the Zeno dynamics[26] in tight-binding lattices do not yield a purely exponential decay of quantum states, and the resulting deviations at short propagation distances[30] can be accounted for by defining effective loss rates $\gamma_{H/V}$ and their respective mean $\bar{\gamma}$ and mismatch $\Delta\gamma$ (see Supplementary Information for details). Figure 3b shows the observed classical intensity distribution excitations after a propagation length of $z = 15$ cm, where a fraction of 48.3% of vertically polarized light has remained in the target waveguide (corresponding to a loss rate of $\gamma_V = 0.02433\,\mathrm{cm}^{-1}$), while the substantially larger coupling in the horizontal polarization component was able to reduce the respective transmission to 4.5% ($\gamma_H = 0.1035\,\mathrm{cm}^{-1}$).

To study the impact on HOM dynamics, a polarization-duplexed two-photon state, with one photon each in the diagonal and anti-diagonal states, was synthesized from a spontaneous parametric downconversion (SPDC) photon-pair source and injected into the target waveguide. At the other end of the sample, a polarization beamsplitter (PBS) served to separate the photons remaining in the target waveguide according to their polarization, and route them to dedicated single-photon counting modules (SPCMs) to register coincidences between the two output ports. Crucially, a half-wave plate (HWP) placed in front of the PBS allowed us to freely choose the orientation θ of the observation polarization between the horizontal/vertical (H/V, $\theta = 0°$) and diagonal/anti-diagonal (D/A, 45°) cases by an appropriate orientation $\theta/2$ of its fast axis (Fig. 4a). In turn, the characteristic HOM patterns were recorded by varying the photons' relative delay τ at the injection facet between $\tau = 0$ for the indistinguishable configuration and $|\tau| > 1$ ps for the fully distinguishable case.

In a first set of experiments we set the birefringence of the target waveguide such that the cumulative phase difference along the sample yielded $\Delta\beta z = 0$ modulo π, meaning that any observed change to the photons' polarization state at the output is directly associated with the respective loss rates $\gamma_{H/V}$ instantiated by the ancillary arrays. Notably, this configuration removes any impact of the polarization coupling dynamics in the target waveguide on the HOM interference, allowing us to directly characterize the influence of observation basis choice. As shown in Fig. 4b for six representative orientation angles θ of the HWP, the obtained HOM pattern can be continually tuned between the conventional HOM dip regime in the H/V basis ($\theta = 0°$) with a visibility of $v_{HV} = -94.6 \pm 1.0\%$, via the case of HOM suppression ($v = 2.9 \pm 0.9\%$ at $\theta = 18°$), to a pronounced HOM peak displaying a visibility of $v_{AD} = +54.1 \pm 0.9\%$ in the A/D basis ($\theta = 45°$). Note that an ideal HOM peak visibility of $v_{AD} = 1$ would be reached in the limiting case of zero transmission in one of

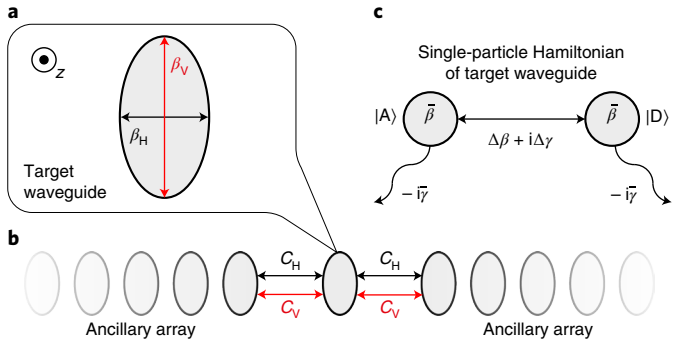

Fig. 2 | Loss implementation in a polarization coupler. a,**b**, When the birefringent target waveguide with propagation constants $\beta_{H/V}$ along its horizontal/vertical principal axes (**a**) is brought into contact with ancillary arrays comprised of tightly coupled waveguides (**b**), the resulting polarization-sensitive coupling strengths C_H and C_V establish polarization-dependent loss rates γ_H and γ_V for the target (central) waveguide. Details on the polarization dependence of coupling are provided in Extended Data Fig. 1. **c**, In the AD-polarization basis, the mean propagation constant $\bar{\beta} = (\beta_V + \beta_H)/2$ and the real part $\Delta\beta = (\beta_V - \beta_H)/2$ of the coupling rate directly result from the waveguide's birefringence, whereas the global loss $\bar{\gamma} = (\gamma_H + \gamma_V)/2$ as well as the imaginary part $\Delta\gamma = (\gamma_H - \gamma_V)/2$ of the coupling arise from the differential losses of the H and V components, respectively. Together, these four quantities make up the non-Hermitian single-particle Hamiltonian of the polarization coupler.

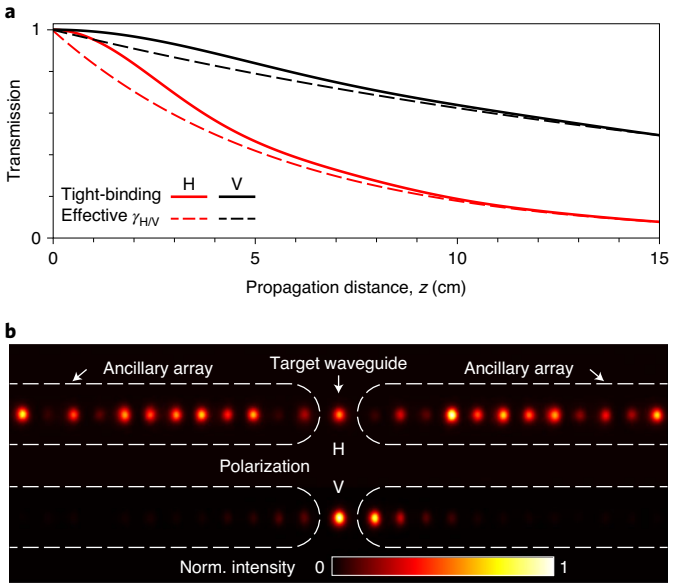

Fig. 3 | Light dynamics under the influence of differential losses. a, Calculated evolution of the probability of photons in H (red) and V (black) polarization remaining in the target waveguide as determined by tight-binding dynamics (solid lines). Provided the intra-array couplings are sufficiently large to efficiently transport the photons away once they have been extracted, the initial Zeno/anti-Zeno dynamics quickly transition into the exponential decay behaviour associated with constant losses. For ease of handling, we employ effective loss rates that yield the same net decays after the sample length of 15 cm (dashed lines). **b**, Normalized output intensity distribution of the system observed with a charge-coupled device camera when the target waveguide is illuminated with appropriate polarized classical light at $\lambda = 814$ nm. Whereas only 4.5% of H-polarized light emerges from the target waveguide at $z = 15$ cm, 48.3% of V-polarized light polarization remains in the target guide. The corresponding effective loss rates are $\gamma_H = 0.1035\,\mathrm{cm}^{-1}$ and $\gamma_V = 0.02433\,\mathrm{cm}^{-1}$, respectively.

the polarizations H or V (Extended Data Fig. 2 presents an equivalent realization of this configuration with a high-contrast polarizer).

To gain a more detailed understanding of the interplay between the choice of basis and the polarization coupling dynamics, we implemented three additional settings: a system with identical losses ($\bar{\gamma} = 0.0639\,\mathrm{cm}^{-1}$, $\Delta\gamma = 0.0396\,\mathrm{cm}^{-1}$) but a non-trivial cumulative phase of $\Delta\beta z = \pi/4$ modulo $\pi/2$, representing a balanced A/D polarization coupler, and the 'lossless' counterparts ($\bar{\gamma} = 0$; that is, in the absence of ancillary arrays) for the cases of $\Delta\beta z = 0$ and $\Delta\beta z = \pi/4$. Figure 4c summarizes the dependence of the visibility on basis orientation and polarization coupling (Extended Data Fig. 3 presents individual basis-dependent HOM traces). Although the A/D basis clearly allows for both HOM dips and HOM peaks to be observed depending on the specific combination of cumulative phase and basis orientation, the H/V basis universally enforces a suppression of the two-photon coincidences ($v_{HV} \approx -1$). This prevalence of the conventional HOM dip is inextricably linked to the structure of the two-photon state

$$\Psi_{ind}(z) = e^{-2i\bar{\beta}z}\left(\frac{e^{-2i\Delta\beta z}e^{-2\gamma_V z}}{\sqrt{2}}|VV\rangle - \frac{e^{-2i\Delta\beta z}e^{-2\gamma_H z}}{\sqrt{2}}|HH\rangle\right). \quad (2)$$

As it evolves from the injected state $\Psi(0) = (|AD\rangle + |DA\rangle)/\sqrt{2} = (|VV\rangle - |HH\rangle)/\sqrt{2}$ by propagating though the system, the bunching of indistinguishable photons in the H and V polarizations is retained, regardless of the propagation phasors $e^{-2i(\bar{\beta}\pm\Delta\beta)z}$ or the specific values of the loss rates $\gamma_{H/V}$. It follows that the indistinguishable photons never coincide in the H/V basis (as indicated in Fig. 1b). By contrast, the two-photon wavefunction of distinguishable particles injected as $|A, D\rangle$ evolves as

$$\Psi_{dis}(z) = e^{-2i\bar{\beta}z}\left(\frac{e^{-2i\Delta\beta z}e^{-2\gamma_V z}}{2}|V, V\rangle + \frac{e^{-(\gamma_V+\gamma_H)z}}{2}(|V, H\rangle - |H, V\rangle) - \frac{e^{2i\Delta\beta z}e^{-2\gamma_H z}}{2}|H, H\rangle\right) \quad (3)$$

and, therefore, yields detectable photon pairs in the states $|V, H\rangle$ and $|H, V\rangle$ for any finite z. In this vein, the impact of non-Hermiticity on the HOM trace is most apparent in the absence of interference terms ($\Delta\beta z = 0$ modulo π). If, in addition, the losses are polarization-independent, that is for a trivial loss mismatch ($\Delta\gamma = 0$), the coincidence rates of distinguishable and indistinguishable particles necessarily coincide and the HOM visibility is suppressed ($v_{AD} = 0$). By contrast, in the limiting case of $\gamma_H \to \infty$, only the first terms of equations (2) and (3) remain: both photons are then V-polarized and register as pairs in the AD basis with a probability of 1/4. Comparing the transmitted amplitudes of the $|VV\rangle$ and $|V, V\rangle$ terms, respectively, one notices that they differ by a factor of $\sqrt{2}$: compared to the baseline of the fully distinguishable case, twice as many indistinguishable photon pairs can, in principle, be observed, corresponding to a HOM peak with ideal maximal visibility of $v_{AD} = 1$, whereas finite loss contrasts yield maximal visibilities in the range of $0 < v_{AD} < 1$ (cf. Fig. 4b, where a maximal visibility of $v_{AD} = 54.1 \pm 0.9\%$ was observed for a loss contrast of $\Delta\gamma = 0.0396\,\mathrm{cm}^{-1}$).

As shown in Fig. 4c, the loss contrast is the crucial variable in determining the specific impact that the HOM interference within the sample has on v_{AD}: the polar plot representation of the visibility landscape depending on θ and $\Delta\beta z$ illustrates that the case of vanishing loss contrast ($\Delta\gamma = 0$, left box) only allows for deviations ($v \approx 0$) from strong suppression ($v \approx -1$) in a narrow region surrounding the AD basis ($\theta = 45°$) for trivial cumulative phases ($\Delta\beta z = 0$). On the other hand, two-photon interference for a bal-

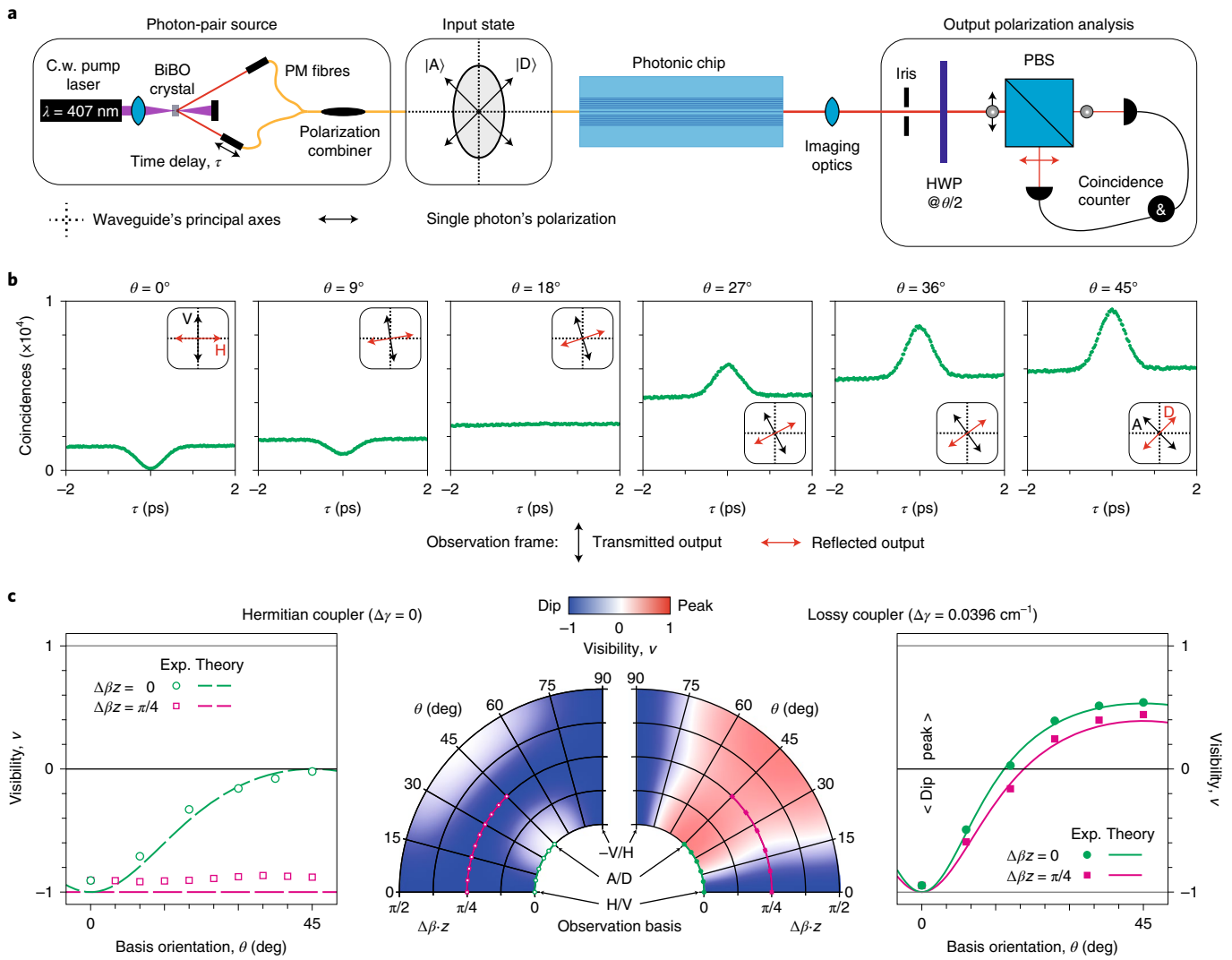

Fig. 4 | Switching between dip and peak in HOM interference. a, Schematic of the experimental set-up. Photon pairs from a type I SPDC source are collected with polarizing fibres and transformed into the desired input state with one photon each in the A and D polarizations by means of a fibre-based polarization combiner. After propagation through the sample, the remaining photons in the target waveguide are analysed with a PBS. Crucially, the orientation angle θ of the basis in which the coincidence counts are detected with SPCMs can be seamlessly adjusted via a HWP. C.w., continuous wave. **b**, HOM patterns recorded in the lossy coupler with $\Delta\beta z = 0$ for different detection basis orientations ranging from the HV ($\theta = 0°$) to the AD orientation ($\theta = 45°$). As a guide to the eye, the basis orientations with respect to the HV frame (dashed lines) are show as red and black arrows. **c**, Calculated (lines) and observed (circles) basis-dependent HOM visibilities in the Hermitian system (left) and under the influence of differential losses (right) for polarization couplers with accumulated phases of $\Delta\beta z = 0$ modulo π (green) and $\Delta\beta z = \pi/4$ modulo $\pi/2$ (magenta). The full set of corresponding experimental HOM traces is shown in Extended Data Fig. 3. The polar plots illustrate the underlying physics by means of colour-encoded HOM visibilities for arbitrary basis orientations $\theta \in [0, 90°]$ and accumulated phases $\Delta\beta z \in [0, \pi/2]$. The green and magenta dashed traces indicate the theory datasets in the adjacent plots.

anced splitting ratio ($\Delta\beta z = \pi/4$) exhibits basis-independent visibilities $v \approx -1$, which also holds for fermionic two-photon states (as calculated in Supplementary Section 3) with visibility $v \approx 1$. By contrast, a non-trivial loss mismatch ($\Delta\gamma = 0.0396\ \mathrm{cm}^{-1}$, right box) leads to nearly $\Delta\beta z$-independent visibilities for any given basis orientation θ. This calculated behaviour is confirmed by the observed visibilities. These measurements clearly show that the requirement of $\Delta\beta z \approx \pi/4$ for quantum interference in the lossless case can be overcome by introducing non-trivial loss contrasts. This confirms that a new mechanism for tailoring two-photon coincidences has indeed been identified.

In conclusion, our findings outline a new approach to manipulate the coincidence dynamics of biphotons through the interplay of non-Hermitian systems and multiple-particle quantum mechanics. To this end, the polarization degree of freedom allows both for a seamless adjustment of the observation basis and for the implementation of complex loss profiles, facilitating a clear distinction between non-Hermitian photon dynamics and the basis-independent HOM visibilities for Hermitian quantum interference. Notably, the techniques described here can be readily combined with the versatility afforded by the three-dimensional spatial arrangement of birefringent waveguides[25], specific exchange symmetries of the input states[31] and waveguide structures in higher synthetic dimensions[6], and open up a number of fascinating opportunities. For example, probabilistic quantum gates clearly stand to benefit greatly from the capability to introduce sophisticated loss realization into integrated optical platforms. Arbitrary quantum-optical transformations such as the singular value decomposition[32] can be emulated in photonic sys-

tems, and even experiments on the evolution of multiple-particle quantum states in complex non-Hermitian systems become experimentally accessible. Taking a broader perspective, the reported basis-sensitive non-classical interference during photon evolution in open systems provides a first glance at previously unexplored physics behind the HOM dip. Along these lines, it will be of particular interest to leverage non-Hermitian HOM interferometry to explore photon-pair evolution in topological edge states[33] and PT-symmetric quantum systems[23], as well as quantum interference phenomena that arise from the Harper–Hofstadter model[34], all of which are brought into experimental reach by our platform[6].

Online content

Any methods, additional references, Nature Research reporting summaries, source data, extended data, supplementary information, acknowledgements, peer review information; details of author contributions and competing interests; and statements of data and code availability are available at https://doi.org/10.1038/s41566-021-00943-3.

Received: 18 May 2021; Accepted: 2 December 2021;
Published online: 7 February 2022

References

1. Fermi, E. Zur Quantelung des idealen einatomigen Gases. *Zeitschrift Phys.* **36**, 902–912 (1926).
2. Dirac, P. A. M. On the theory of quantum mechanics. *Proc. R. Soc. Lond. A* **112**, 661–677 (1926).
3. Bose, S. N. Plancks Gesetz und Lichtquantenhypothese. *Zeitschrift Phys.* **26**, 178–181 (1924).
4. Bose, S. N. Wärmegleichgewicht im Strahlungsfeld bei Anwesenheit von Materie. *Zeitschrift Phys.* **27**, 384–393 (1924).
5. Hong, C. K., Ou, Z. Y. & Mandel, L. Measurement of subpicosecond time intervals between two photons by interference. *Phys. Rev. Lett.* **59**, 2044–2046 (1987).
6. Ehrhardt, M. et al. Exploring complex graphs using three-dimensional quantum walks of correlated photons. *Sci. Adv.* **7**, eabc5266 (2021).
7. Vest, B. et al. Anti-coalescence of bosons on a lossy beam splitter. *Science* **356**, 1373–1376 (2017).
8. Wolterink, T. A. W. et al. Programmable two-photon quantum interference in 10^3 channels in opaque scattering media. *Phys. Rev. A* **93**, 53817 (2016).
9. Crespi, A. et al. Particle statistics affects quantum decay and Fano interference. *Phys. Rev. Lett.* **114**, 090201 (2015).
10. Bender, C. M. & Boettcher, S. Real spectra in non-Hermitian Hamiltonians having PT symmetry. *Phys. Rev. Lett.* **80**, 5243–5246 (1998).
11. Makris, K. G., El-Ganainy, R., Christodoulides, D. N. & Musslimani, Z. H. Beam dynamics in PT symmetric optical lattices. *Phys. Rev. Lett.* **100**, 103904 (2008).
12. El-Ganainy, R. et al. Non-Hermitian physics and PT symmetry. *Nat. Phys.* **14**, 11–19 (2018).
13. Rüter, C. E. et al. Observation of parity-time symmetry in optics. *Nat. Phys.* **6**, 192–195 (2010).
14. Eichelkraut, T. et al. Mobility transition from ballistic to diffusive transport in non-Hermitian lattices. *Nat. Commun.* **4**, 2533 (2013).
15. Guo, A. et al. Observation of PT-symmetry breaking in complex optical potentials. *Phys. Rev. Lett.* **103**, 093902 (2009).
16. Regensburger, A. et al. Parity-time synthetic photonic lattices. *Nature* **488**, 167–171 (2012).
17. Miri, M. A. & Alù, A. Exceptÿional points in optics and photonics. *Science* **363**, eaar7709 (2019).
18. Hodaei, H. et al. Enhanced sensitivity at higher-order exceptional points. *Nature* **548**, 187–191 (2017).
19. Feng, L., Wong, Z. J., Ma, R. M., Wang, Y. & Zhang, X. Single-mode laser by parity-time symmetry breaking. *Science* **346**, 972–975 (2014).
20. Hodaei, H., Miri, M. A., Heinrich, M., Christodoulides, D. N. & Khajavikhan, M. Parity-time-symmetric microring lasers. *Science* **346**, 975–978 (2014).
21. Weidemann, S. et al. Topological funneling of light. *Science* **368**, 311–314 (2020).
22. Scheel, S. & Szameit, A. PT-symmetric photonic quantum systems with gain and loss do not exist. *Europhys. Lett.* **122**, 34001 (2018).
23. Klauck, F. et al. Observation of PT-symmetric quantum interference. *Nat. Photon.* **13**, 883–887 (2019).
24. Li, Q. et al. A non-unitary metasurface enables continuous control of quantum photon–photon interactions from bosonic to fermionic. *Nat. Photon.* **15**, 267–271 (2021).
25. Szameit, A. & Nolte, S. Discrete optics in femtosecond-laserwritten photonic structures. *J. Phys. B* **43**, 163001 (2010).
26. Longhi, S. Nonexponential decay via tunneling in tight-binding lattices and the optical zeno effect. *Phys. Rev. Lett.* **97**, 110402 (2006).
27. Biggerstaff, D. N. et al. Enhancing coherent transport in a photonic network using controllable decoherence. *Nat. Commun.* **7**, 11282 (2016).
28. Rojas-Rojas, S. et al. Analytical model for polarization-dependent light propagation in waveguide arrays and applications. *Phys. Rev. A* **90**, 063823 (2014).
29. Longhi, S. Quantum statistical signature of PT symmetry breaking. *Opt. Lett.* **45**, 1591–1594 (2020).
30. Dreisow, F. et al. Decay control via discrete-to-continuum coupling modulation in an optical waveguide system. *Phys. Rev. Lett.* **101**, 143602 (2008).
31. Sansoni, L. et al. Two-particle bosonic-fermionic quantum walk via integrated photonics. *Phys. Rev. Lett.* **108**, 010502 (2012).
32. Tischler, N., Rockstuhl, C. & Słowik, K. Quantum optical realization of arbitrary linear transformations allowing for loss and gain. *Phys. Rev. X* **8**, 021017 (2018).
33. Tambasco, J. L. et al. Quantum interference of topological states of light. *Sci. Adv.* **4**, eaat3187 (2018).
34. Tai, M. E. et al. Microscopy of the interacting Harper–Hofstadter model in the two-body limit. *Nature* **546**, 519–523 (2017).

Methods

Waveguide fabrication and birefringence characterization. We used the femtosecond-laser direct-writing technique[25] to inscribe systems of evanescently coupled single-mode waveguides. To this end, ultrashort laser pulses with 270-fs duration at a carrier wavelength of $\lambda = 517$ nm and a repetition rate of 333 kHz from a fibre amplifier system (Coherent Monaco) were focused into the bulk of 150-mm-long fused-silica samples (Corning 7980) through a ×50 objective (NA = 0.60), forming waveguides along desired trajectories by translating the sample with a precision positioning system (Aerotech ALS180).

The combination of elliptical material modifications with residual stress fields from the rapid quenching immediately following the inscription pass imbues the laser-written waveguides with an inherent birefringence, the strength of which can be tuned via the writing speed[35]. We characterized the waveguides using classical light and crossed polarizers[36]. Having placed the sample between two PBSs and simultaneously rotating them by an angle φ (while maintaining their respective crossed orientation), the ratio of the transmitted (I_T) and total intensities (I_{total}) was measured with two photodiodes and evaluated according to the theoretical model

$$\frac{I_T}{I_{total}} = \sin^2(2\varphi)\sin^2(\Delta\beta z),$$

allowing for the relevant values of 0 and $\pi/4$ of the cumulative phase difference $\Delta\beta z$ to be identified by $\max(I_T/I_{total}) = 0.5$ and $\max(I_T/I_{total}) = 0$ up to multiples of $\pi/2$ and π, respectively.

For our experiments we chose a separation of 27.5 µm between the target waveguide and the ancillary arrays, corresponding to coupling strengths of $C_H = 0.154\,\mathrm{cm}^{-1}$ and $C_V = 0.065\,\mathrm{cm}^{-1}$ of the polarization eigenstates to their respective 'sinks'. To ensure that photons, once extracted from the target guide, were swiftly transported away, an array pitch of 20 µm was used to set the intra-array coupling strengths to $0.551\,\mathrm{cm}^{-1}$ and $0.335\,\mathrm{cm}^{-1}$ for the horizontal and vertical polarizations, respectively (see Extended Data Fig. 1 for more details on the dependence of the coupling strength on polarization and waveguide separation).

Biphoton creation and detection. For the generation of photon pairs, we used a type I SPDC source (Fig. 4a). A bismuth borate (BiBO) crystal was pumped by a 100-mW continuous-wave laser diode (Coherent OBIS) at $\lambda = 407$ nm, producing wavelength-degenerate horizontally polarized photon pairs at $\lambda = 814$ nm, which were subsequently collected by polarizing fibres and routed to the sample via a polarization combiner with adjustable principal axes of the output fibre. A variable delay τ between the arrival times of the two photons at the sample was implemented by means of a motorized translation stage (PI). The degree of indistinguishability of the photons was characterized by recording the HOM dip with a fibre-based beamsplitter, yielding a visibility of up to $v = -97.2 \pm 1.1\%$. To record coincidences, the single photons at the output of the PBS were detected with SPCMs (Excelitas Technologies, detection efficiency of >50%, dark counts of $<50\,\mathrm{s}^{-1}$, dead time of 20 ns), the signals of which were processed with a correlation card (Becker & Hickl).

Data availability

All experimental data that have been used to produce the results reported in this manuscript are available in an open-access data repository[37].

References

35. Yang, P., Burns, G. R., Guo, J., Luk, T. S. & Vawter, G. A. Femtosecond laser-pulse-induced birefringence in optically isotropic glass. *J. Appl. Phys.* **95**, 5280–5283 (2004).
36. Heilmann, R., Gräfe, M., Nolte, S. & Szameit, A. Arbitrary photonic wave plate operations on chip: realizing Hadamard, Pauli-X, and rotation gates for polarisation qubits. *Sci. Rep.* **4**, 4118 (2014).
37. Ehrhardt, M., Heinrich, M. & Szameit, A. Data set for observation-dependent suppression and enhancement of two-photon coincidences by tailored losses. Rostock University Publication Server https://doi.org/10.18453/rosdok_id00003360 (2021).

Acknowledgements

We thank C. Otto for preparing the high-quality fused-silica samples used in this work. We acknowledge funding from the European Research Council (grant no. 899368 'EPIQUS'), Deutsche Forschungsgemeinschaft (grants nos. SCHE 612/6-1, SZ 276/12-1, BL 574/13-1, SZ 276/15-1 and SZ 276/20-1) and the Alfried Krupp von Bohlen and Halbach Foundation.

Author contributions

M.E. fabricated the samples and carried out the measurements. All authors jointly interpreted the measured data and co-wrote the manuscript.

Funding

Open access funding provided by Universität Rostock.

Competing interests

The authors declare no competing interests.

Additional information

Extended data is available for this paper at https://doi.org/10.1038/s41566-021-00943-3.

Supplementary information The online version contains supplementary material available at https://doi.org/10.1038/s41566-021-00943-3.

Correspondence and requests for materials should be addressed to Alexander Szameit.

Peer review information *Nature Photonics* thanks Yuri Kivshar and the other, anonymous, reviewer(s) for their contribution to the peer review of this work.

Reprints and permissions information is available at www.nature.com/reprints.

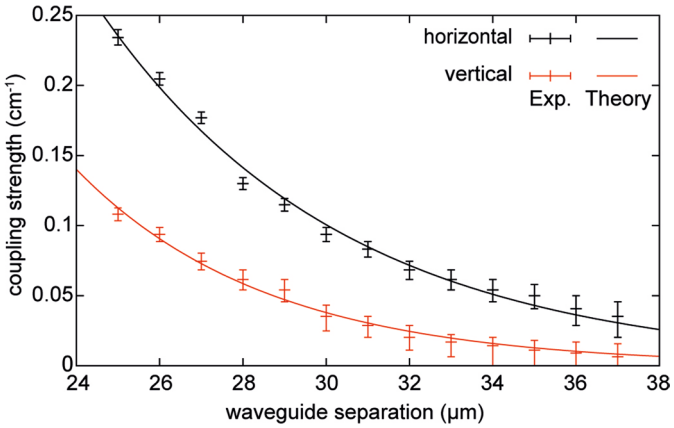

Extended Data Fig. 1 | Dependence of the coupling strength on distance and polarization. Horizontally/vertically polarized classical light at a wavelength of $\lambda = 814$ nm excites appropriately spaced waveguide pairs in order to calibrate the coupling strength from the waveguides' output intensities.

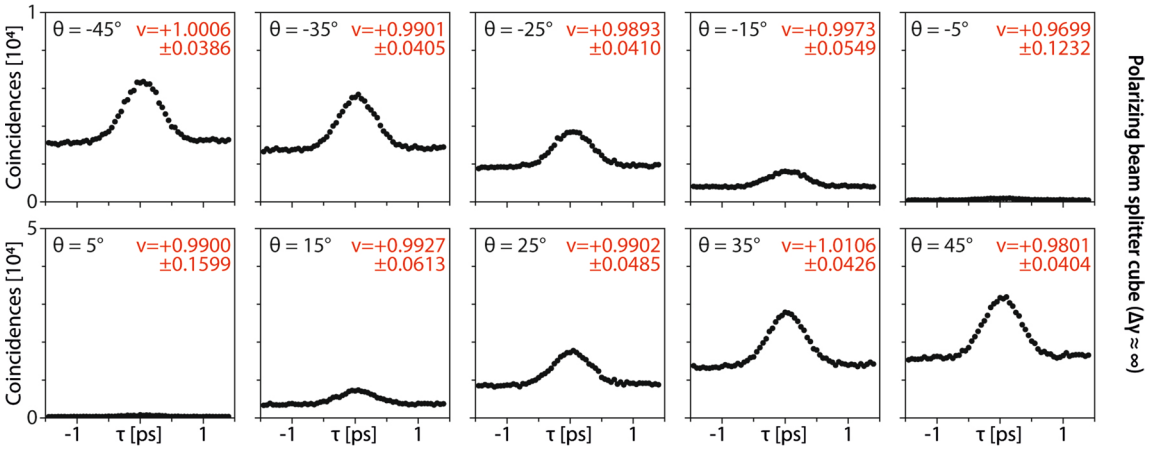

Extended Data Fig. 2 | HOM traces in the strongly non-Hermitian limit. These HOM traces are observed by replacing the birefringent photonic chip with a standard polarizing beam splitter cube with an intensity extinction ration of 10^3 between H and V polarization, corresponding to the limit of $\Delta\gamma \to \infty$. In accordance with the calculated behavior, shown in Supplementary Information, the peak visibility remains near unity irrespective of the basis orientation, while the overall count rate is maximal in the AD basis ($\theta=\pm45°$) and approaches zero in the HV configuration ($\theta=0°$).

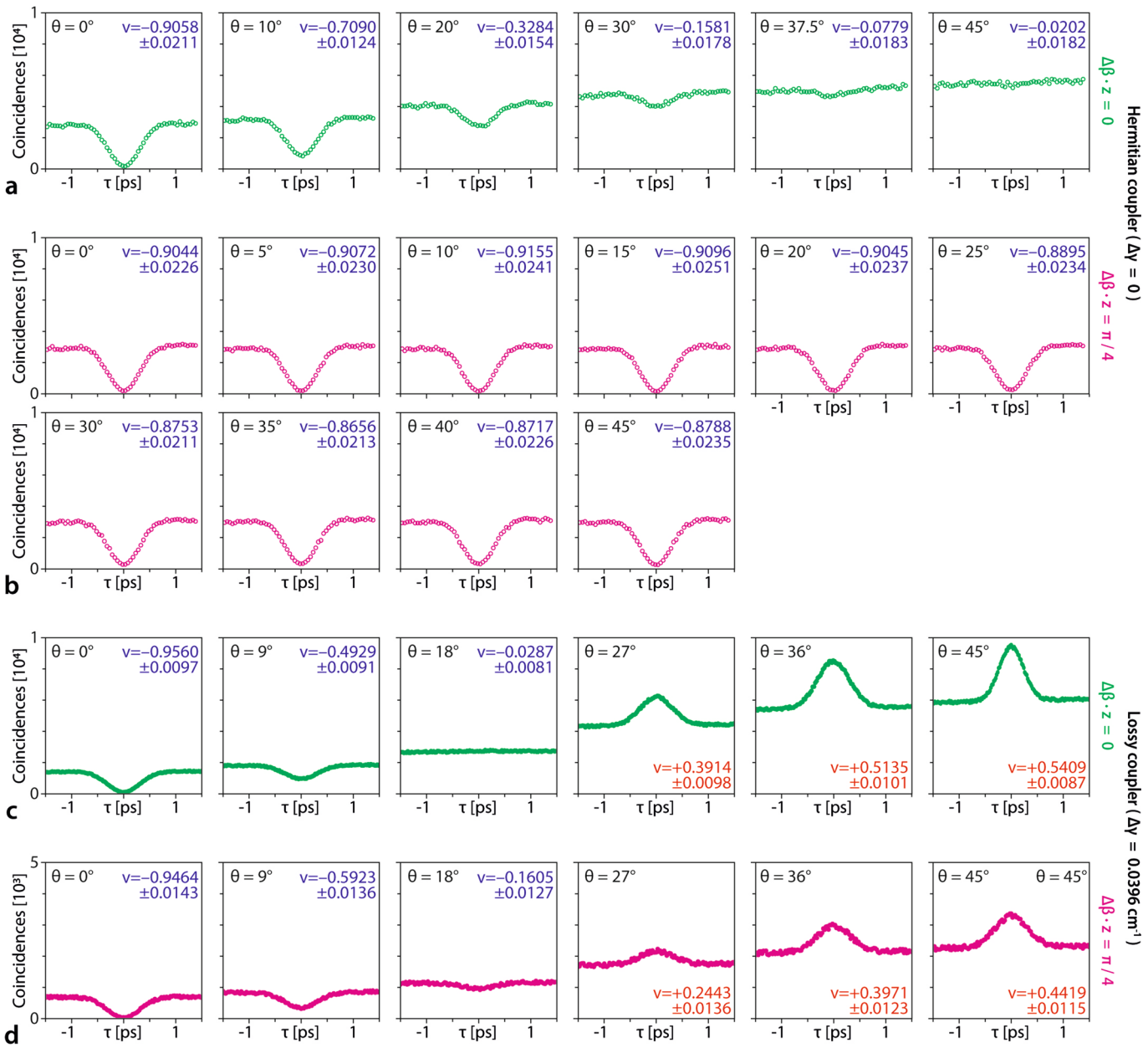

Extended Data Fig. 3 | Full set of measured HOM traces. These HOM pattern are corresponding to the visibilities in Fig. 4c: Hermitian polarization coupler **a** without ($\Delta\beta z = 0$) and **b** with interference ($\Delta\beta z = \pi/4$), and lossy coupler ($\Delta\gamma = 0.0396\,\mathrm{cm}^{-1}$) **c** without ($\Delta\beta z = 0$) and **d** with interference ($\Delta\beta z = \pi/4$), respectively. Note that the data shown in Fig. 4b of the main manuscript is reproduced here in subfigure **b** for ease of comparison with the other configurations.